Influence of Homogenization of Alkali-Activated Slurry on Mechanical Strength

Barbara Horvat, Mark Češnovar, Katja Traven, Majda Pavlin, Katja König, Vilma Ducman

Slovenian National Building and Civil Engineering Institute, Ljubljana, Slovenia
barbara.horvat@zag.si, mark.cesnovar@zag.si, katja.traven@zag.si, majda.pavlin@zag.si, ketsi.koenig@gmail.com, vilma.ducman@zag.si

Abstract Alkali-activated materials are promising materials for the construction industry due to the accessibility of the precursors, which are mainly secondary industrial by-products, and their cost-effective and energy-efficient production. Although these materials are not new, some of the parameters in the technological process are not yet fully understood and tested. Therefore, in this paper in the means of mechanical strength, the preparation of alkali-activated pastes by using a three-roll mill homogenization method is discussed. The influence of homogenization of alkali-activated slurry has been evaluated on different waste materials (fly ash, fly ash with metakaolin, slag mixture (electric arc furnace slag and ladle slag), glass wool, waste green ceramics), which are treated with different alkali activators (NaOH, commercial sodium silicate solution, laboratory-produced alkali activators based on waste cathode- ray tube glass) with different curing regimes (60 °C and 70 °C) and different drying methods (drying at room temperature, drying at 105 °C). The viscosity of the slurry before homogenization was higher than after homogenization, the distribution of elements was more uniform and the compressive strength higher in all homogenized alkali activated materials, regardless of other parameters.

Keywords:
secondary raw material, alkali activated material, foaming, homogenization, mechanical strength

University of Maribor Press

DOI https://doi.org/10.18690/um.fkkt.2.2022.2
ISBN 978-961-286-598-6

1 Introduction

Alkali activation is a chemically driven process in which aluminosilicate-rich precursors react with alkali media to form a solid binder, making these materials one of the promising alternatives to ordinary Portland cement (Juenger et al., 2011). As aluminosilicates are one of the most common minerals in the earth's crust (Schlesinger, 1991), they are contained in clays, in industrial by-products such as biomass and coal fly ashes, metallurgical slags, red mud and mineral wool waste, which offers the possibility to produce sustainable non-structural materials. The alkali-activated materials produced from these precursors have high mechanical strength, high thermal and chemical resistance and are refractory (Bernal and Provis, 2014). One of the possibilities, due to their thermal stability, are prefabricated lightweight insulation boards (foams). The chemical reaction of the so-called alkali activation begins with the dissolution of the aluminosilicates and ends with solidification. Nowadays, it is more often used in the laboratory than on the construction site, because the process is not well understood and the technology is not set up in the same way as for ordinary cement concrete mixtures. Nevertheless, some projects, such as E-crete™, have already shown some of the advantages of using alkali activated materials based on fly ash and slag for pavements: along the freeway in Port Melbourne, precast slabs for VicRoads, which have a much higher strength (55 MPa) than required by governmental legislation (Van Deventer et al., 2012). Therefore, low carbon awareness, a source of precursors and activators with developed technology, and the durable end product for larger-scale production are crucial for production on a larger scale.

Numerous articles are published each year, where alkali activation focuses on the phase composition associated with the type of Ca-containing precursor and a sufficient amount of reactive amorphous Al and Si, computer modelling of the Al:Si ratio, the type and amount of activator, knowing that this is the most important factor in producing a material with the desired microstructure and mechanical properties (Vlček et al., 2014). Although some authors also study in detail the precursor preparations (drying, grinding and sieving) (Traven et al., 2019) and curing regimes (Češnovar et al., 2019) there is no real research in the technology of mixing and homogenizing with alkali activation. Size distribution, shape and packing of the precursor particles during mixing play an important role in the rheology of the alkali-activated slurry (Hunger and Brouwers, 2009). The surface tension of the particle-

fluid interface and the ionic strength of the solution (Provis et al., 2010) is also related to the processability of the slurry. One of the possibilities to solve this problem is the use of chemical admixtures or so-called superplasticisers as used for Portland cement pastes but the results are not yet promising (Criado et al., 2009).

Another possibility to achieve better processability of alkali activated slurries is the correct homogenization. This technique offers the possibility of wetting solid particles while the liquid to dry content is not changed, which is important when the activator to precursor ratio is fixed at a calculated value. In most cases, homogenization is done after addition of an activator to the precursor (or vice versa), by manual mixing for 1 to 5 min by hand (with palate knife) (Rajamma et al., 2012), or mechanically with a laboratory mixer (Korat and Ducman, 2017), with an ordinary mixer for cement pastes such as Automix (Samson et al., 2017), Hobart mixer (Nematollahi et al., 2017) or a combination of mixing by hand and with a mixer (Hajimohammadi et al., 2017). However, when homogenization technology is used, there is still no known relationship with the final mechanical properties of alkali-activated materials. When producing alkali-activated materials on a large scale, preparation of mixtures by manual mixing is impossible due to the longer time required for this process, and manual mixing itself does not provide good and efficient homogenization. This paper tries to clarify how different precursors behave when slurries are mixed manually and/or with laboratory mixers and when a three-roll homogenizer homogenizes them. The homogenization of alkali activated foams based on electric arc furnace slag and fly ash, which are foamed with Na-perborate or H_2O_2, is also investigated. In the production of alkali-activated foams, surface agents such as triton, sodium oleate, sodium dodecyl sulfate or others are added to the slurry to stabilize air voids which are formed by a chemical reaction from the foaming agent (Korat and Ducman, 2017). While foaming and surface agents appear in a solid or liquid state, this also affects the viscosity and workability of the slurry. For foams produced by manual or machine homogenization, different combinations of foaming agent (solid, liquid) and surface agent (solid, liquid) are therefore used.

2 Materials and Methods

2.1 Analysis of precursors and their alkali-activated counterparts

Fly-ash (FA) (Traven et al., 2020), labelled 10 01 01, from Šoštanj power thermoplant, slag mixture (SM) (Češnovar et al., 2019), labelled 10 09 031, electric arc furnace slag from SIJ Acroni and ladle slag from SIJ Ravne, while glass wool waste (GW) (Horvat et al., 2018), labelled 17 09 041, and green waste ceramics (GWC) (Horvat and Ducman, 2019), labelled 10 12 011, were collected from Termit. The samples of all waste materials were collected in a way that is representative for landfills.

The metakaolin used in experiments (MK; Argeco) (Kramar et al., 2016; Provis et al., 2019) was used in the RILEM project and is not waste material.

X-ray fluorescence was performed on melted discs (XRF; Thermo Scientific ARL Perform'X Sequential XRF) prepared with $Fluxana_{(s)}$ (FX-X50-2, lithium tetraborate 50% / lithium metaborate 50%) to lower melting point and with the addition of $LiBr_{(l)}$ (prepared from 50 ml H_2O and 7.5 g of $LiBr_{(s)}$ from Acros Organics) to avoid sticking of the melt to the platinum vessel. The measured data were characterized by the UniQuant 5 software.

The X-ray powder diffraction (XRD; Empyrean PANalytical X-ray Diffractometer, Cu X-ray source) was solved with the software X'Pert Highscore plus 4.1. The Rietveld refinement was performed using an external standard (a pure Al_2O_3 crystal) to estimate the amount of amorphous phase and minerals in waste materials.

All samples used for XRF and XRD were dried at 70 °C for 24 h (WTB binder), ground with the vibrating disk mill (Siebtechnik) and sieved below 63 μm (SM), 90 μm (FA, GW and WGC).

The viscosity of alkali-activated slurries (a mixture of precursor, alkali activator and potential foam stabilizing additives) was measured with the viscometer Haake VT 500 with the detector PK2-1° (measurable viscosity range for this detector is from 0.04 Pa·s to 400 Pa·s) at 25 °C.

Fourier transform infrared spectroscopy (FTIR; PerkinElmer Spectrum Two) was performed on non-homogenized and homogenized alkali activated fly ash.

Scanning electron microscopy (SEM; Jeol JSM-IT500) to investigate surface, shape and microstructure was performed under high vacuum conditions on dried precursors and alkali-activated samples, both sputtered with Au. Energy-dispersive X-ray spectroscopy (EDXS; Oxford Instruments, Link Pentafet) mapping was performed on polished, non-sputtered, alkali-activated samples in low vacuum conditions. All alkali-activated samples for the analysis of SEM were dried in vacuum at 40 °C for 24 h (Kambič, VS 50 S).

The surface of a cross-section of polished vacuumed alkali-activated samples was also examined with a digital microscope (Tagarno FHD Trend) and software (Tagarno measuring software). Due to the sensitivity during polishing, especially of foam, the polishing was performed gently by hand.

Measurements of bending and compressive strength of alkali activated materials and foam were carried out with compression and bending strength testing machine (ToniTechnik ToniNORM) 1 day after demoulding unless otherwise stated.

The geometric density of alkali-activated samples was determined by weighting the sample and dividing its mass by its volume.

2.2 Preparation of precursors, activator and alkali-activated samples

All precursors used for alkali activation shown in Fig. 1 were prepared as shown:

- FA: used as received;
- FA*: FA and MK were used as received. Both precursors were mixed in mass ratio 3:1 respectively;
- SM: crushed in the gyratory crusher (Retsch BB50), ground in vibrating disk mill (Siebtechnik), sieved below 63 μm. Afterwards, both slags were mixed in mass ratio 1:1;
- GW: drying at 70 °C for 24 h, ground in cement mixer using iron balls and sieved below 63 μm;

– WGC: drying at 70 °C for 24 h, ground with a pestle and mortar and sieved below 1 mm.

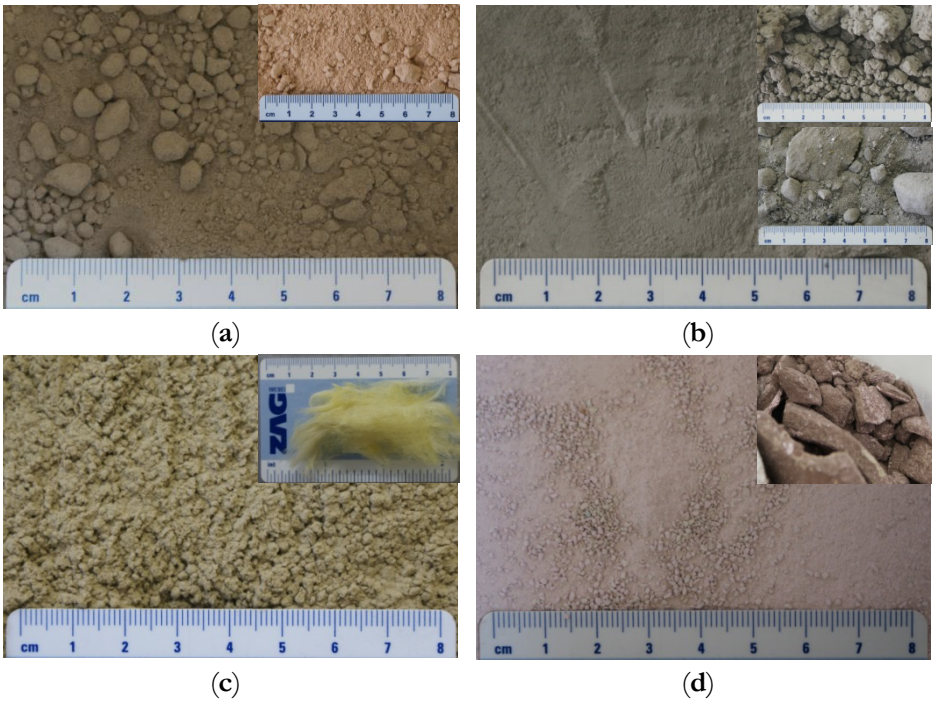

Figure 1: Photograph of precursors' state used in alkali activation: (a) FA, on the inset, is MK (larger particles fall apart when touched), (b) SM, (c) GW and (d) WGC. On the insets are photographs of the virgin material: (b-up) electric arc slag, (b-down) ladle slag, (c) GW, (d) WGC.

Surce: own.

For the alkali reaction versatile alkali activators were produced and/or used:

– FA: Alkali activator has been produced using ground glass powder (cathode ray tube waste glass) with an average particle size below 90 μm. After boiling for 6 h to 45 h, the prepared suspensions were filtered and the filtrates were analysed for silicon and aluminium content with an inductively coupled plasma optical emission spectrometer (ICP-OES, Varian, Model 715-ES): mass percentage of Na_2O 0.02%, the mass percentage of SiO_2 2.32%, and mass percentage of Al_2O_3 0.073%);

- FA*: Na-water glass "Crystal" (Crystal, 0112, Tennants distribution, with the mass percentage of Na_2O 18.8%, and mass percentage of SiO_2 37.0%) and $NaOH_{(s)}$ (Donau Chemie Ätznatron Schuppen, EINECS 215-785-5);
- SM: Na-water glass "Crystal" (Crystal, 0112, Tennants distribution, with a mass percentage of Na_2O 18.8%, and the mass percentage of SiO_2 37.0%);
- GW: Na-water glass "Termit" (Silvez, mining company Termit, with the mass percentage of Na_2O 12.8%, and mass percentage of SiO_2 29.2%) and $NaOH_{(s)}$ (Donau Chemie Ätznatron Schuppen, EINECS 215-785-5);
- WGC: Na-water glass "Geosil" (Geosil, 344/7, Woelner, with the mass percentage of Na_2O 16.9%, and the mass percentage of SiO_2 27.5%.

Preparation of alkali slurry:

- FA: precursor was manually mixed for 1 min with manually premixed alkali activator in mass ratio 3.37:1 respectively;
- FA*: precursor was manually mixed for 1 min with manually premixed alkali activators (Na-water glass "Crystal" and $NaOH_{(s)}$), foaming agent (H_2O_2, Carlo Erba reagents) and stabilizing agent (Na-dodecyl sulphate, Acros Organics) in mass ratio 2.66:1:0.05:0.04:0.04 respectively. The time of the start of the foaming reaction was estimated from the observation of bubble formation on the surface and volume growth;
- SM: precursor was manually mixed with manually premixed alkali activator (Na-water glass "Crystal"), foaming agent (Na-perborate monohydrate$_{(s)}$; Belinka Perkemija d.o.o.) and stabilizing agent (triton$_{(l)}$; X-100 Electrophoresis, Dow Chemical Company) in mass ratio 1.89:1:0.06:0.03 respectively. The time of the start of the foam reaction was estimated from the observation of bubble formation on the surface and volume growth;
- GW: precursor was mixed (up to 1000 rpm for 1 min with mixer Tehtnica Železniki, UM-405) with manually premixed alkali activators (Na-water glass "Termit" and $NaOH_{(s)}$) in the mass ratio 1.28:1:0.05 respectively;
- WGC: precursor was mixed (up to 1000 rpm for 1 min with mixer Tehtnica Železniki, UM-405) with alkali activator (Na-water glass "Geosil") in mass ratio 1.35:1 respectively.

Half of each slurry was homogenized in a three-roll mill (Exakt 80S) until the slurries did not change their visual texture.

All slurries were put into rubber-silicon moulds of size (80x20x20) mm^3 and cured (WTB Binder):

- FA: at 70 °C for 72 h;
- FA*: at 70 °C for 72 h;
- SM: at 60 °C for 24 h;
- GW: at 60 °C for 24 h;
- WGC: at 70 °C for 24 h.

Demoulding and drying process before measuring the mechanical strength:

- FA: the prisms were demoulded after cooling to room temperature and left at room temperature for an additional 24 h;
- FA*: the prisms were demoulded after cooling to room temperature and left at room temperature for an additional 24 h;
- SM: the prisms were demoulded after cooling to room temperature and right after the mechanical properties were measured;
- GW: the prisms were demoulded after cooling to room temperature and right after the mechanical properties were measured;
- WGC: the prisms were demoulded 3 weeks after curing at 70 °C and heat-treated at 105 °C for the additional 24 h (WTB Binder) because they were still not fully solidified.

3 Results and discussion

3.1 Analysis of precursor

SEM micrographs of all precursors prepared for alkali activation are shown in Fig. 2 under lower and higher magnification. FA consists of typical spheres (Fig. 2 (a) and (b)) (Kutchko and Kim, 2006), FA* from FA and large aggregates from MK (Fig. 2 (c) and (d)), GW from elongated cylindrical structures (Fig. 2 (g) and (h)), which are also longer than 63 μm (size of the mesh used), while both SM (Fig. 2 (e)

and (f)) and WGC (Fig. 2 (i) and (j)) come from randomly shaped particles with sharp edges by grinding.

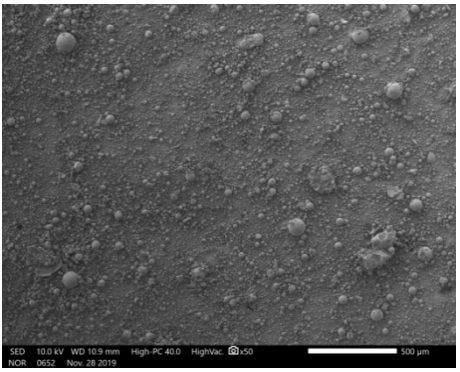

(**a**)

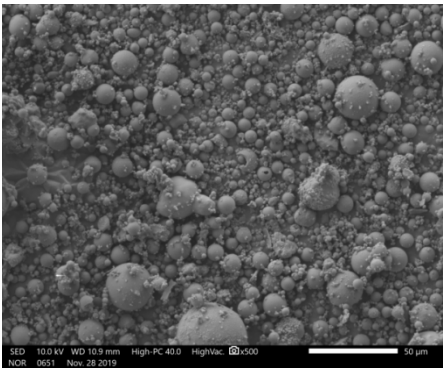

(**b**)

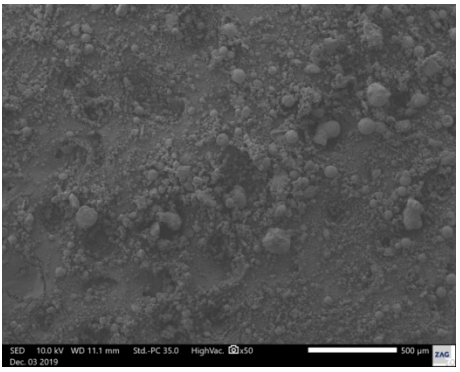

(**c**)

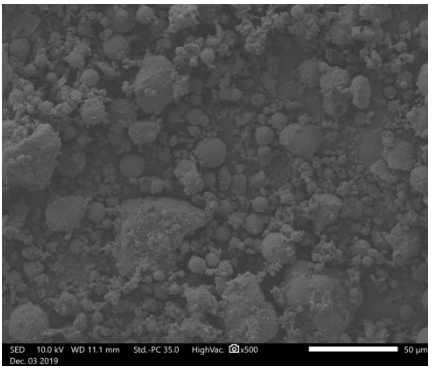

(**d**)

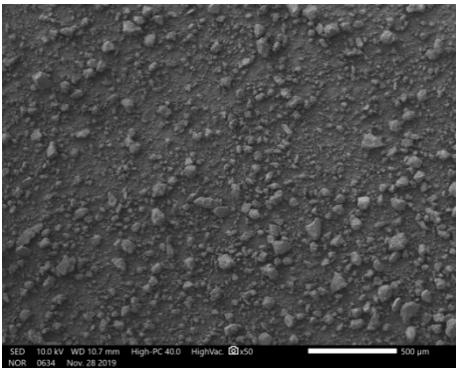

(**e**)

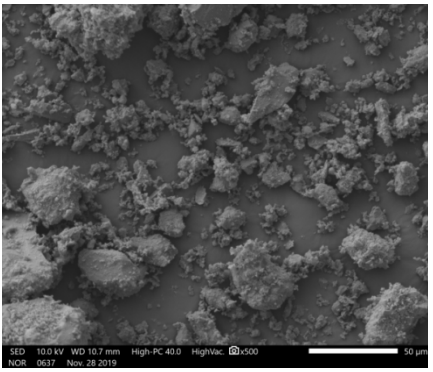

(**f**)

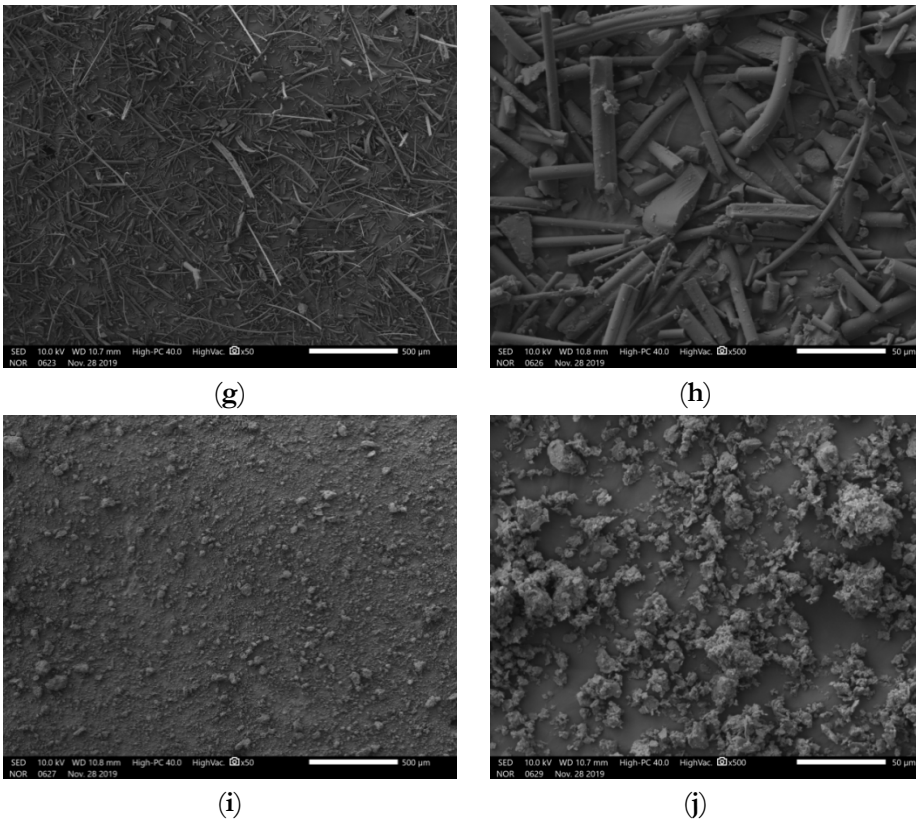

Figure 2: SEM micrographs of FA [(a) magnification 50x, (b) magnification 500x], FA* [(c) magnification 50x, (d) magnification 500x], SM [(e) magnification 50x, (f) magnification 500x], GW [(g) magnification 50x, (h) magnification 500x] and WGC [(i) magnification 50x, (j) magnification 500x].

Surce: own.

The chemical analysis of the precursor is presented in Table 1, with the first row of each precursor showing the mass percentages of elements detected by XRF, and the second row showing the mass percentages of elements in the crystalline phase determined by Rietveld refinement on XRD patterns, and in the third line, the mass percentages of the elements in the amorphous phase are shown, calculated as the difference between the amount of the mass percentage of an element determined using XRD and the mass percentage of an element in the crystalline phase.

Table 1: The first row of each precursor shows the mass percentage of elements measured by XRF, the second row shows the mass percentage of elements in a crystalline phase determined by Rietveld refinement from XRD, and the third row shows the mass percentage of elements in the amorphous phase.

Precursor	Elements/m%	Na	K	Cs	Mg	Ca	Sr	Ba	Al	Si
FA	XRF	0.89	1.83	0	1.69	8.85	0.05	0.07	12.16	20.91
	XRD	0	0	0	0.38	1.64	0	0	1.74	4.32
	XRF-XRD	0.89	1.83	0	1.31	7.21	0.05	0.07	10.42	16.59
FA*	XRF	0.66	1.41	0	1.30	6.72	0.04	0.06	12.50	23.85
	XRD	0	0	0	0.39	1.33	0	0.01	1.56	7.12
	XRF-XRD	0.66	1.41	0	0.91	5.39	0.04	0.05	10.94	16.73
SM	XRF	0.23	0.17	0	14.28	21.58	0.04	0.03	4.47	9.87
	XRD	0	0	0	5.43	11.12	0	0.02	1.07	6.03
	XRF-XRD	0.23	0.17	0	8.85	10.46	0.04	0.01	3.40	3.84
GW	XRF	12.24	0.29	0	2.22	5.10	0	0.06	1.32	30.73
	XRD	0	0	0	0.18	0.54	0	0	0	2.61
	XRF-XRD	12.24	0.29	0	2.03	4.56	0	0.06	1.31	28.12
WGC	XRF	0.25	3.66	0	0.87	2.41	0.02	0.36	12.24	28.76
	XRD	0	0	0	0.72	2.41	0	0	4.02	14.81
	XRF-XRD	0.25	3.66	0	0.15	0	0.02	0.36	8.22	13.95

The optimum ratio of the amount of substance in the alkaline activated final sample is $n_{Na+K}:n_{Al}:n_{Si}=1:1:1.9$ (Duxson et al., 2005), which was experimentally proven in our investigations at the WGC, where we only considered elements in the amorphous phase (Horvat and Ducman, 2019). An increased ratio (normalized to the amount of substance Al), where the whole first and second group of the periodic system are taken into account ($n_{1st}:n_{2nd}:n_{Al}:n_{Si}$), is for precursors:

- FA: 0.22:0.61:1:1.53;
- FA*: 0.16:0.43:1:1.47;
- SM: 0.11:4.97:1:1.09;
- GW: 11.05:4.05:1:20.57;
- WGC: 0.34:0:1:1.64.

If only elements from the first group of the periodic system are considered, for FA, FA* (addition of MK to FA lowered amounts of elements from the first and second group, and lowered ratio Si:Al), SM and GWC addition of Na (element of the first group) and Si is required, which can be both added with Na-water glass and a potentially insufficient amount of Na with NaOH, while in GW too much Na (to avoid efflorescence) is present even without alkali activator, i.e. GW can only be used as an additive to other precursors.

If elements from the second group are also considered, it is noticeable that FA, FA* and SM contain more amorphous elements from the second group than from the first group. When considering that 1 element from the second group can compensate "wrong" Al charge in the matrix for 2 Al, the normalized amount of substance of Al that can be compensated from both cationic groups present in the precursor is:

- FA: 1.44;
- FA*: 1.02;
- SM: 10.05;
- GW: 19.15;
- WGC: 0.68.

From the above list, it can be concluded that the addition of cations from alkali activators to the precursors FA, FA*, SM and GW lead to efflorescence because the final normalized (normalization to the amount of substance for Al) amount of substance of the cations should have the value 1 (this value is already higher for the precursor without alkali additives alone). The only precursor with a lower substance quantity of the first and second group before the addition of alkali activators is the WGC, which is the only precursor among the selected precursors, with which efflorescence can be avoided if the alkali activators are selected correctly if minerals found in precursors with XRD (Fig. 3) do not dissolve in alkali.

- Fig. 3 shows the XRD measurements of all precursors and their Rietveld refinement results (the GOF value of all analyzed samples was below 10 - the value is higher because the precursors are (mostly) waste products and several peaks on the XRD samples could not be determined and are contained in the amount of the amorphous phase). The highest amount of amorphous phase is GW (90%), followed by FA (80%), FA* (70%), WGC (50%) and SM (40%). The higher amount of amorphous phase can lead to a higher amount of aluminosilicate network in the final alkaline activated material. Minerals that are detected with XRD when they do not react with alkali or become unstable at the curing temperature represent aggregates of different Mohs hardness in the final product, i.e. when they have a higher hardness than the alkaline activated sample has higher compressive strength

(Horvat and Ducman, 2019). The only mineral present in all precursors is quartz, which accounts for a higher mass percentage in all precursors used (Fig. 3).

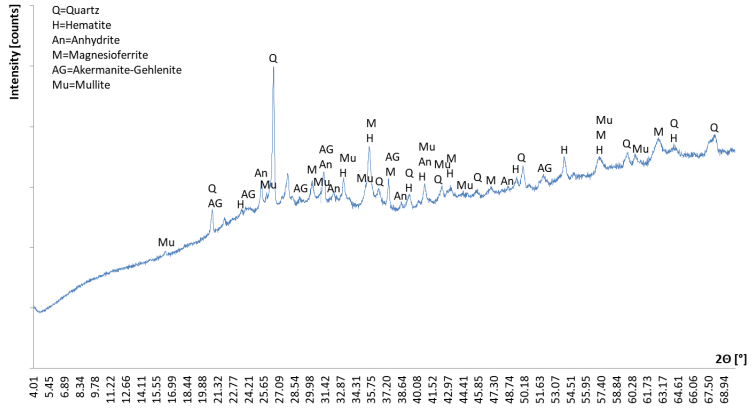
Q=Quartz
H=Hematite
An=Anhydrite
M=Magnesioferrite
AG=Akermanite-Gehlenite
Mu=Mullite
Intensity [counts]
2Θ [°]

(a)

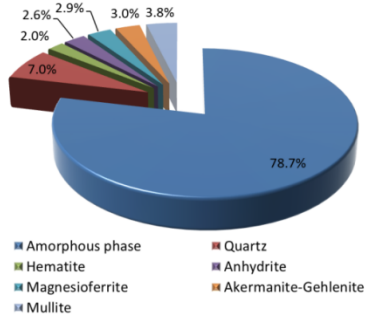
2.6%
2.9%
3.0%
3.8%
2.0%
7.0%
78.7%
Amorphous phase
Quartz
Hematite
Anhydrite
Magnesioferrite
Akermanite-Gehlenite
Mullite

(b)

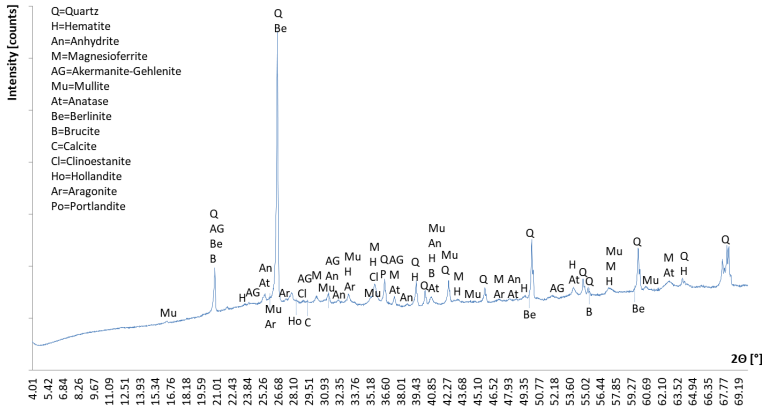
Q=Quartz
H=Hematite
An=Anhydrite
M=Magnesioferrite
AG=Akermanite-Gehlenite
Mu=Mullite
At=Anatase
Be=Berlinite
B=Brucite
C=Calcite
Cl=Clinoestanite
Ho=Hollandite
Ar=Aragonite
Po=Portlandite
Intensity [counts]
2Θ [°]

(c)

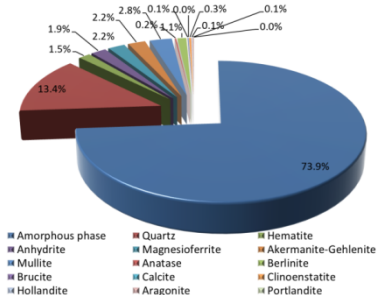
1.9%
2.2%
2.8%
0.1%
0.0%
0.3%
0.1%
1.5%
2.2%
0.2%
1.1%
0.1%
0.0%
13.4%
73.9%
Amorphous phase
Quartz
Hematite
Anhydrite
Magnesioferrite
Akermanite-Gehlenite
Mullite
Anatase
Berlinite
Brucite
Calcite
Clinoenstatite
Hollandite
Aragonite
Portlandite

(d)

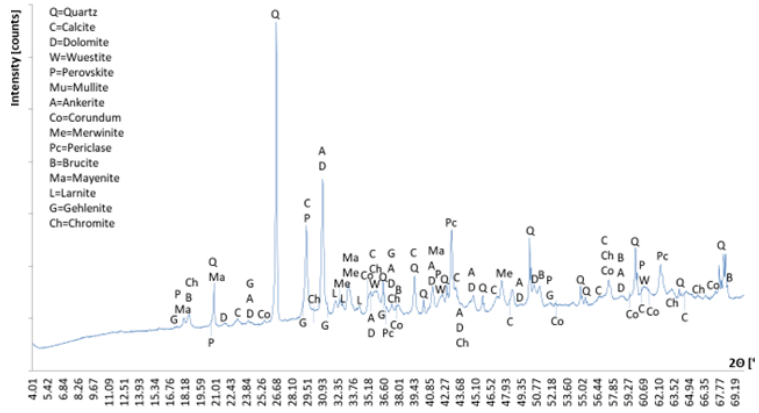
Q=Quartz
C=Calcite
D=Dolomite
W=Wuestite
P=Perovskite
Mu=Mullite
A=Ankerite
Co=Corundum
Me=Merwinite
Pc=Periclase
B=Brucite
Ma=Mayenite
L=Larnite
G=Gehlenite
Ch=Chromite
Intensity [counts]
2θ [°]

(e)

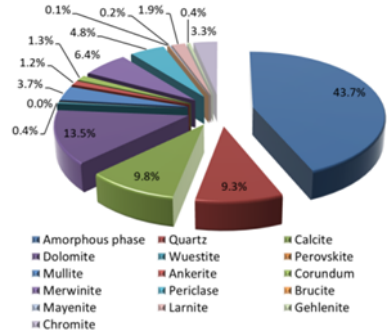
43.7%
9.3%
9.8%
13.5%
0.4%
0.0%
3.7%
1.2%
1.3%
6.4%
4.8%
0.1%
0.2%
1.9%
0.4%
3.3%
Amorphous phase
Quartz
Calcite
Dolomite
Wuestite
Perovskite
Mullite
Ankerite
Corundum
Merwinite
Periclase
Brucite
Mayenite
Larnite
Gehlenite
Chromite

(f)

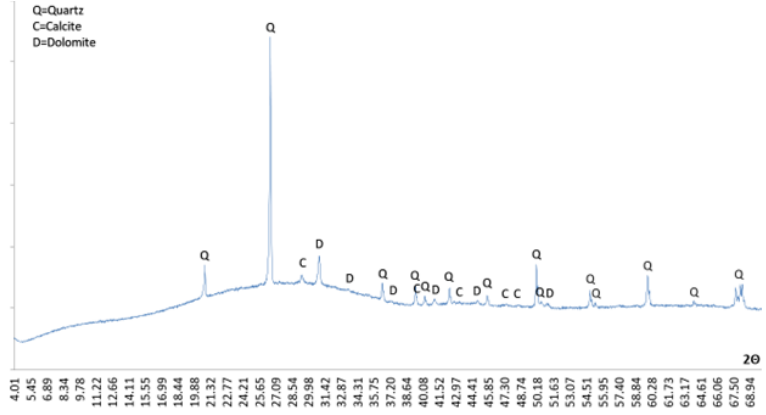
Q=Quartz
C=Calcite
D=Dolomite
2θ

(g)

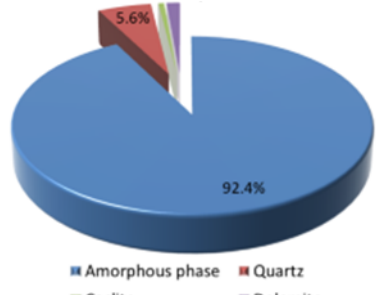
92.4%
5.6%
Amorphous phase
Quartz

(h)

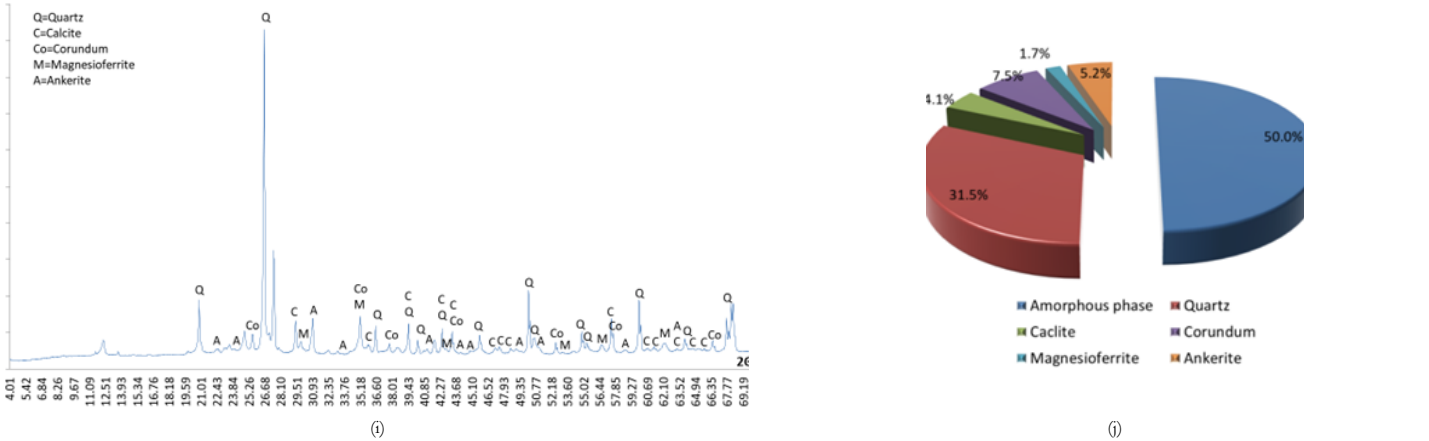

(i) (j)

Figure 3: XRD pattern of (a) FA, (c) FA*, (e) SM, (g) GW and (i) GWC. Rietveld refinement of (b) FA, (d) FA*, (f) SM, (h) GW and (j) GWC.
Source: own.

3.2 Analysis of alkali-activated samples

During homogenization of FA slurry gas (white-grey smoke) was produced, while during homogenization of other mixtures slurries became visually just smoother and easier to handle.

The compressive and flexural strength of all alkaline activated samples produced from homogenized and non-homogenized slurries are shown in Table 2 together with the viscosity of the slurries and the density of the final products. The viscosity decreases with homogenization from high to measurable high for alkaline activated material from GW, for alkaline activated materials from FA for 55% and from WGC for 60%, for alkaline activated foams from FA* for 15% and from SM for 30%. The compressive strength was increased for all tested samples, i.e. for alkaline activated materials from GW by 25%, from FA by 55% and from WGC by 70%, for alkaline activated foams from FA* by 75% and SM by 50%. The flexural strength was also increased for all samples tested, i.e. for alkaline activated materials from GW by 10%, from FA by 30% and from WGC by 80%, for alkaline activated foams from FA* by 100% and from SM from non-existent to 10% of the value of the flexural strength of alkaline activated material from GW.

Table 2: The density of alkali-activated samples, their compressive and bending strengths in the dependence of preparation of alkali slurry, with and without (intact) homogenization.

Precursor	Preparation of the slurry	Viscosity of the slurry/ Pa·s	Compressive strength/ MPa	Bending strength/ MPa	Density/ kg/l
FA	Intact	5.03	30.25	7.20	1.71
	Homogenization	2.23	46.76	9.46	1.77
FA*	Intact	0.90	3.23	2.11	0.70
	Homogenization	0.75	5.67	4.27	0.84
SM	Intact	1.08	0.92	0	0.64
	Homogenization	0.76	1.38	1.71	0.64
GW	Intact	torque overload	54.91	14.00	1.75
	Homogenization	41.13	69.87	15.86	1.79
WGC	Intact	6.43	11.03	9.05	1.87
	Homogenization	2.55	19.00	16.13	1.35

Mechanical strength of alkali-activated foams increased less if foaming did not start too early because the homogenization did not influence the foaming of the slurry, i.e. final density of alkali-activated foam did not change, the material was just homogenized in its pre-foaming time (SM was foamed with Na-perborate which started to foam approximately 5 min after precursor was mixed with foaming and stabilizing agent, i.e. after 1 min of mixing there were still approximately 4 min for homogenization and moulding), i.e. under the digital microscope, there was no obvious difference in pore size and distribution with and without homogenization (Fig. 4 (e) and (f) respectively).

If foaming started during homogenization, gas bubbles were removed from the slurry mechanically and final density of the alkali-activated foam was higher due to homogenization and gas bubble-removal (FA* was foamed with H_2O_2 which started to react during 1 min time of mixing of the precursor with foaming and stabilizing agent, i.e. homogenization and moulding do influence final properties of the foam). Homogenization during foaming also affected bubble distribution and size, i.e. homogenized sample has smaller, more uniformly sized and more uniformly distributed pores, as it is presented on Fig. 4 (c) and (d), i.e. sample without and with homogenization respectively.

Bloating of WGC occurred during drying at 110 °C and was more pronounced when the material was homogenized (Fig. 4 (j)), due to the alkali activation of the whole material, while non-reacted precursors were observed with intact alkali-activated material (light pink and white-yellow particles in Fig. 4 (i); the alkali did not reach the inner volume of the particles of the precursor, which were additionally crushed and dispersed with homogenization). One consequence of the bloating was a decrease in density of almost 30%, which has a negative effect on mechanical strength, i.e. an increase in bending and mechanical strength of homogenized material dried by methods that avoid bloating would result in an even greater increase in mechanical strength. Figure 4: Microphotographs of vacuumed polished alkali-activated samples' cross-sections performed with a digital microscope at magnification 25 for FA [(a) intact, (b) homogenized], FA* [(c) intact, (d) homogenized], SM [(e) intact, (f) homogenized], GW [(g) intact, (h) homogenized] and WGC [(i) intact, (j) homogenized].

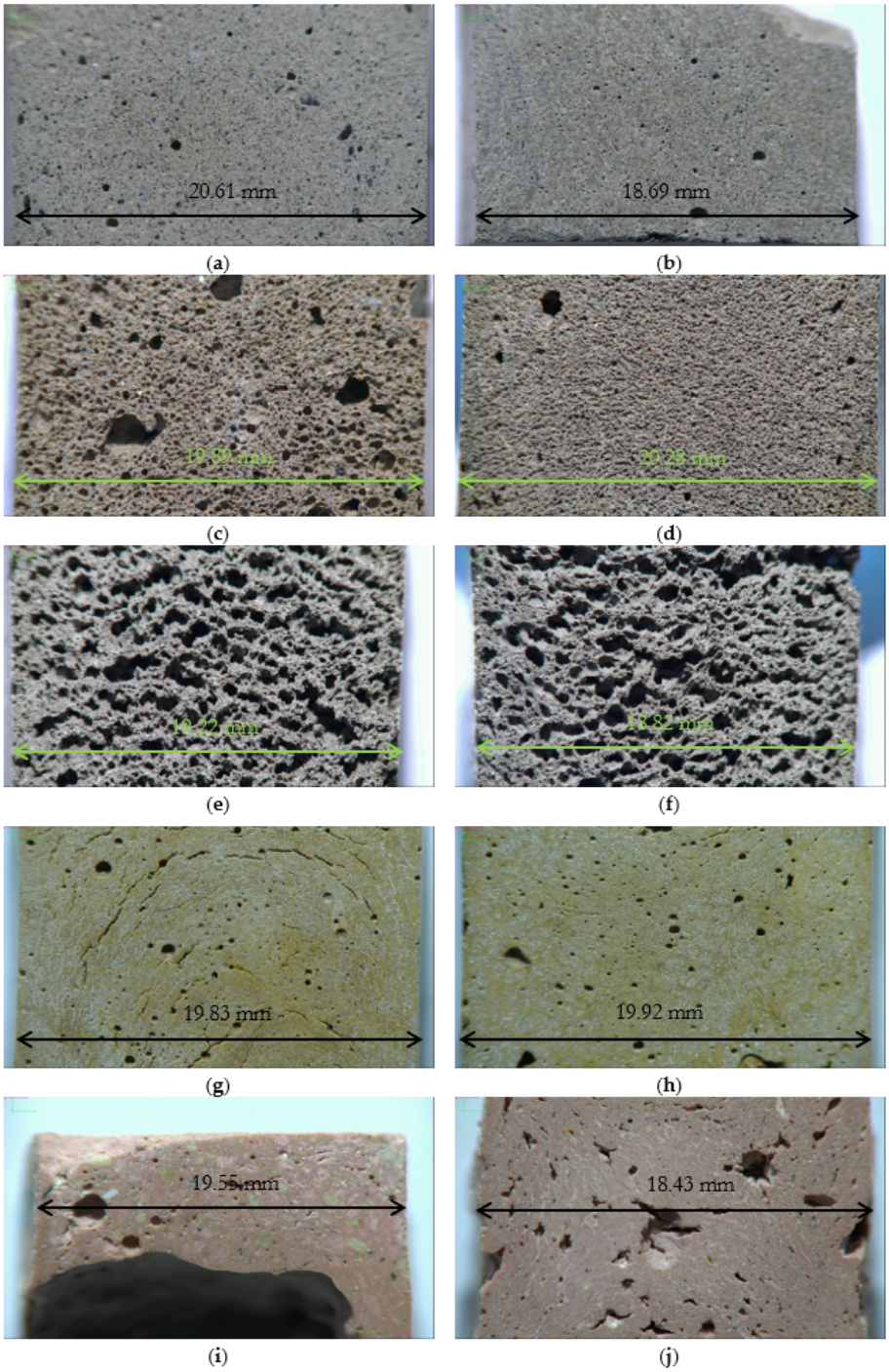
20.61 mm
(a)
18.69 mm
(b)
19.59 mm
(c)
20.28 mm
(d)
19.42 mm
(e)
18.82 mm
(f)
19.83 mm
(g)
19.92 mm
(h)
19.55 mm
(i)
18.43 mm
(j)

Figure 4: Microphotographs of vacuumed polished alkali-activated samples' cross-sections performed with a digital microscope at magnification 25 for FA [(a) intact, (b) homogenized], FA* [(c) intact, (d) homogenized], SM [(e) intact, (f) homogenized], GW [(g) intact, (h) homogenized] and WGC [(i) intact, (j) homogenized]

Alkali-activated GW without homogenization showed circular longitudinal pores (Fig. 4 (g)), which are a consequence of manual moulding of slurry that is too viscous (almost as bulk material), whereas these pores are not observed in homogenized alkali-activated GW (Fig. 4 (h)), therefore, the higher mechanical strength of the homogenized sample. FA Alkali-activated without homogenization contains larger black, non-spherical particles that are not present in the homogenized sample (Fig. 4 (a) and (b) respectively).

Fig. 5 shows intact alkali-activated FA and Fig. 6 shows homogenized alkali-activated FA.

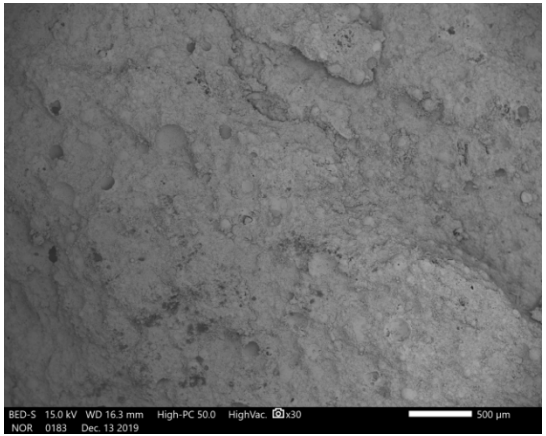

(**a**)

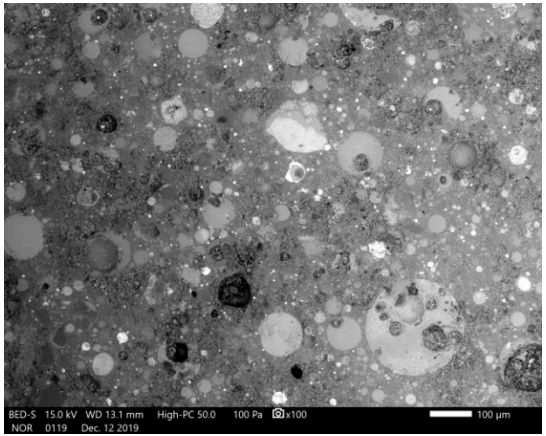

(**b**)

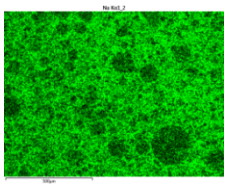

(b-Na)

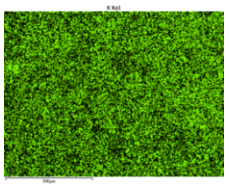

(b-K)

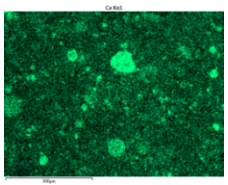

(b-Ca)

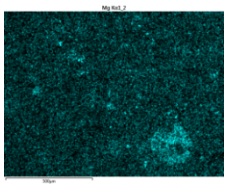

(b-Mg)

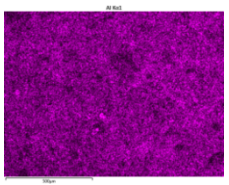

(b-Al)

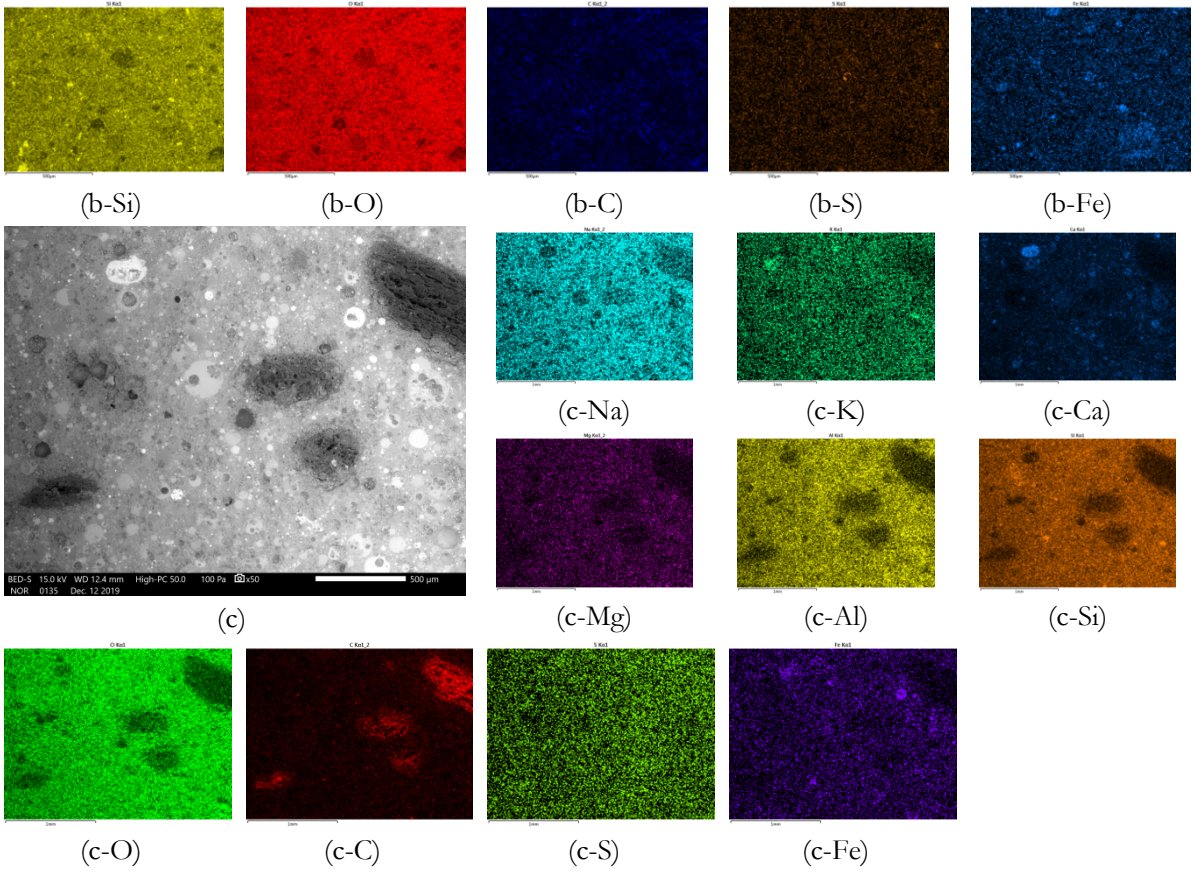

Figure 5: SEM micrograph of intact alkali-activated FA with magnification (a) 30 (intact cross-section after compressive strength test, vacuumed and sputtered with Au, observed at HV), (b) 100 and (c) 50 (cut and polished cross-section, observed at LV). The EDXS mapping of micrograph (b), (c) is presented on (b-chemical element), (c-chemical element) respectively.
Source: own.

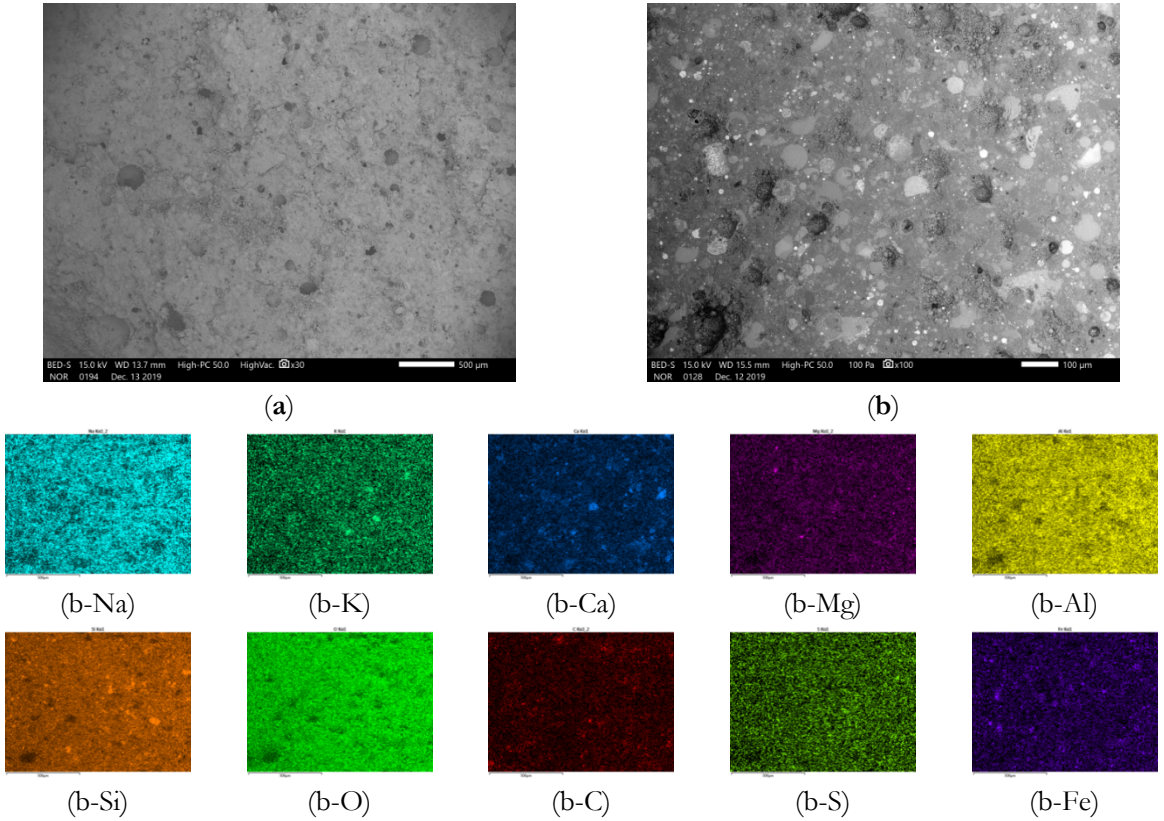

Figure 6: SEM micrograph of homogenized alkali-activated FA with magnification (a) 30 (intact cross-section after compressive strength test, vacuumed and sputtered with Au, observed at HV) and (b) 100 (cut and polished cross-section, observed at LV). The EDXS mapping of micrograph (b) is presented on (b-chemical element). Source: own.

Fig. 5 (a) and Fig. 6 (a) show that there is no difference in the aluminosilicate network, its polished counterparts in Fig. 5 (b) and Fig. 6 (b) show that homogenization led to the grinding of large fly ash spheres that consist from elements of the second group, which were not reacted according to the EDXS analysis, which is beneficial to the product since this improved the ratio of the first and second group to Al, which means that efflorescence could be avoided or at least minimized.

In an intact alkali-activated FA network, incompletely burned organic parts of coal and wood were trapped (Fig. 5 (c)), which were not visible in the homogenized sample. These parts look black to the naked eye under an optical microscope (Fig. 4 (a)) and also under SEM (Fig. 5 (c)), made of C according to EDXS analysis (Fig. 5 (c-C)).

From all EDXS mappings of intact and homogenized alkali-activated FA (Fig. 5 and Fig. 6), it can be concluded that the homogenization also led to a better uniformity of all elements in the alkali-activated sample.

Fig. 7 shows the FTIR analysis of intact and homogenized alkali-activated FA. C-C bonds are present in the intact sample (bands around 1450 cm^{-1} and 890 cm^{-1} belong to the stretching and bending of C-C bonds (Ahmed et al., 2013)), while they have disappeared in the homogenized sample, which proves that the emission of smoke from the slurry during homogenization was the result of the combustion of cellulose (observed under SEM only in intact alkali-activated FA samples, shown in Fig. 5(c)) from the incomplete combustion of coal and wood.

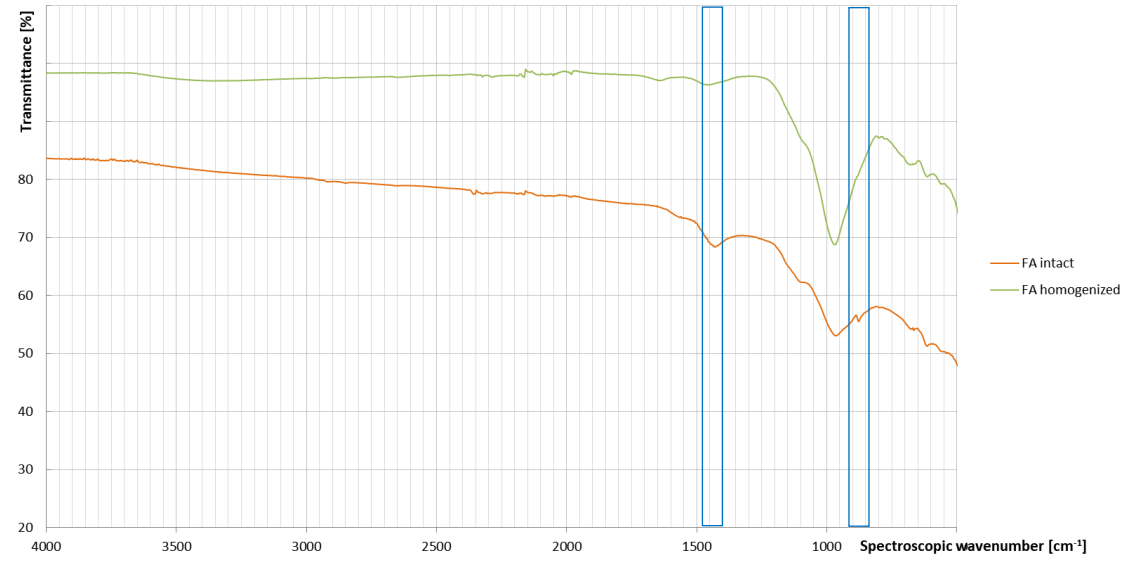

Figure 7: Photo FTIR spectra of intact (orange line) and homogenized (green line) FA.
Source: own.

Fig. 8 shows intact alkali-activated FA* and Fig. 9 shows homogenized alkali-activated FA*:

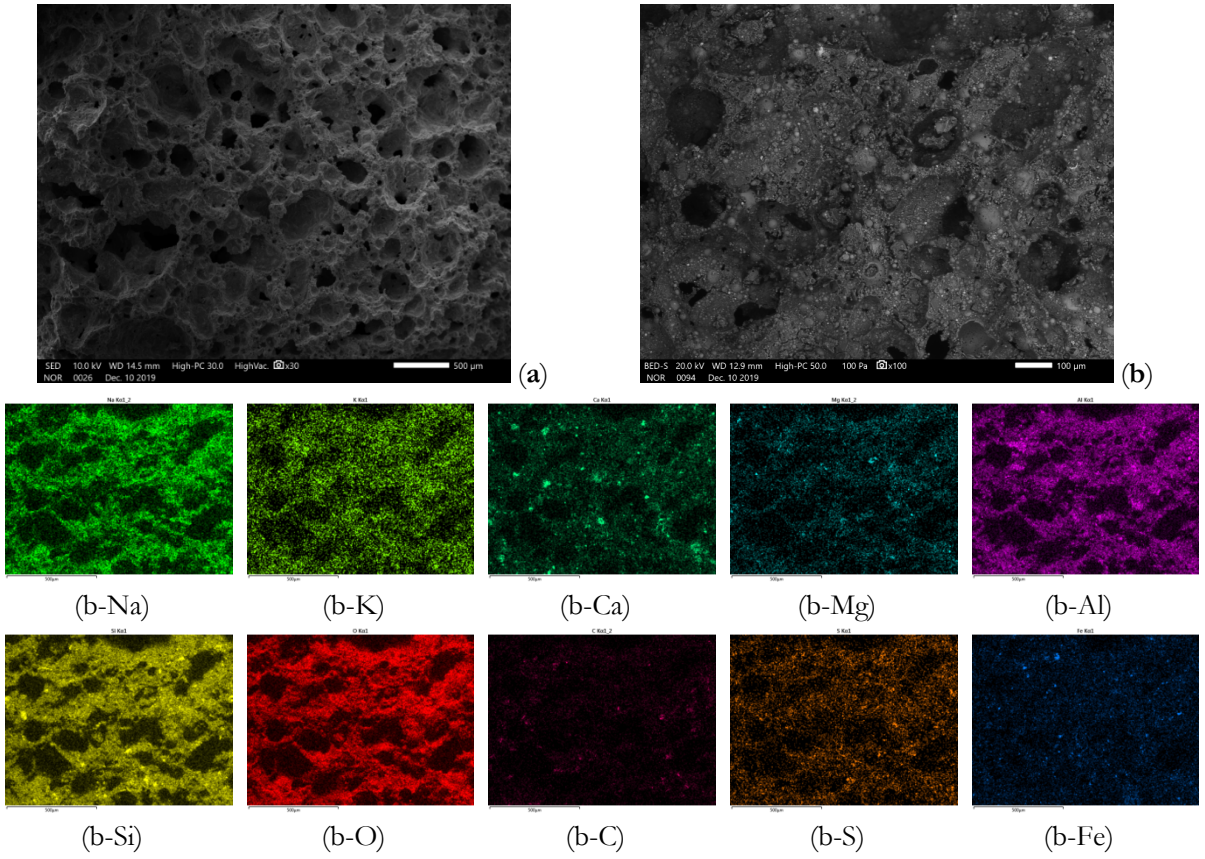

Figure 8: SEM micrograph of intact alkali-activated FA* with magnification (a) 30 (intact cross-section after compressive strength test, vacuumed and sputtered with Au, observed at HV) and (b) 100 (cut and gently polished cross-section, observed at LV). The EDXS mapping of micrograph (b) is presented on (b-chemical element). Source: own.

When comparing Fig. 8 (a) and Fig. 9 (a), it becomes clear that the aluminosilicate network shows no visible change, while the pores are more uniform in size and more uniformly distributed after homogenization. The mean value of pore size from SEM micrographs of intact alkali-activated FA* is 240.4 μm (standard deviation 173.7 μm), while the mean value for homogenized alkali-activated FA* is 98.9 (standard deviation 40.4 μm). The value decreased by 60% and the pores are more homogeneously distributed according to the decrease of the standard deviation (4-times) compared to the mean value of the pore diameter (2-times).

From the EDXS analysis of alkali-activated FA* polished counterparts (shown in Fig. 8 (b) and Fig. 9 (b)), it is the same as for the alkali-activation of FA (Fig. 5 and Fig. 6), i.e. spheres from elements from the second group did not react and are simply ground after homogenization, which leads to a better element distribution over the entire alkali-activated FA* (Fig. 8 (b-element) and Fig. 9 (b-element)).

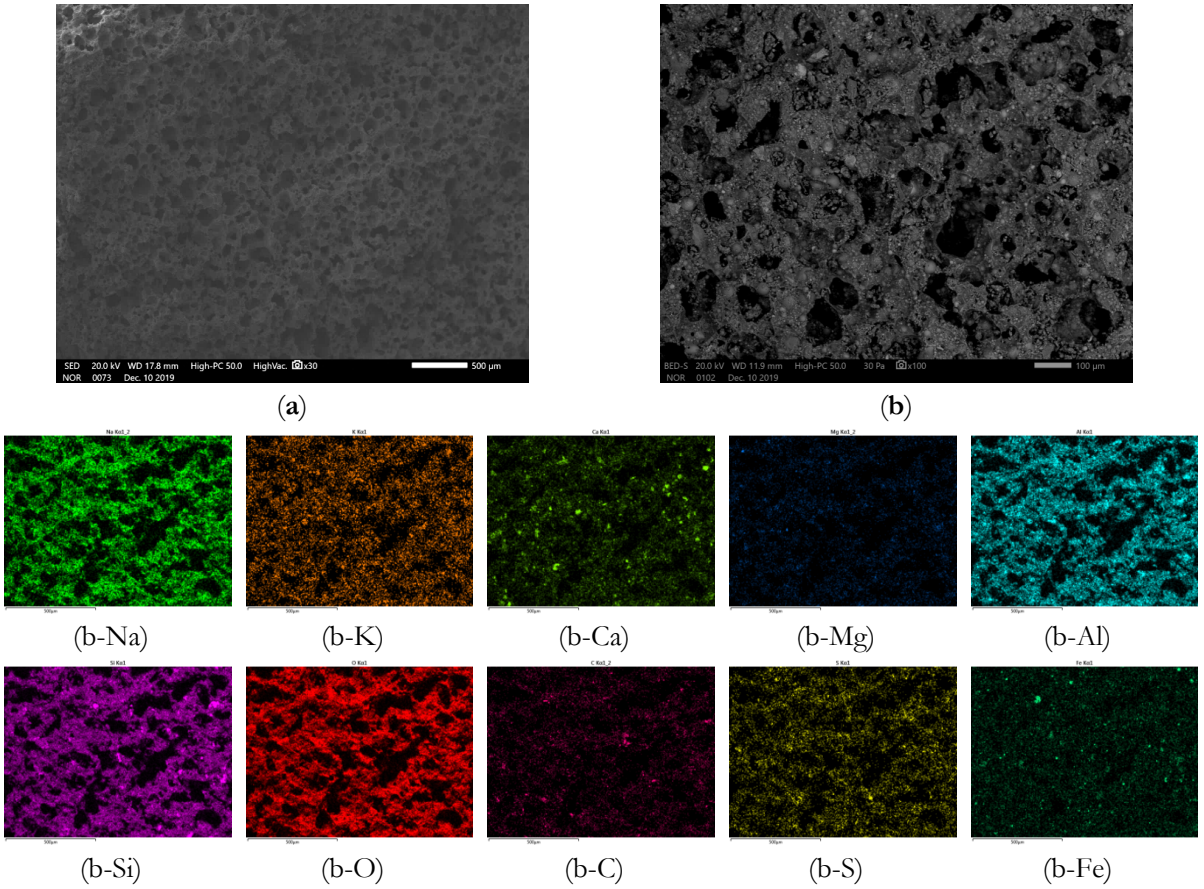

Figure 9: SEM micrograph of homogenized, alkali-activated FA* with magnification (a) 30 (intact cross-section after compressive strength test, vacuumed and sputtered with Au, observed under HV) and (b) 100 (cut and gently polished cross-section, observed under LV). The EDXS mapping of the micrograph (b) is presented under (b-chemical element). Source: own.

Fig. 10 shows intact alkali-activated SM and Fig. 11 shows homogenized alkali-activated SM. The aluminosilicate network before and after homogenization of SM presented in Fig. 10 (a) and Fig. 11 (a) shows no change. The statistics of the measured pores on SEM micrographs show that the mean value of the pore size of intact, alkali-activated SM is 533.8 μm (standard deviation 275.1 μm), while the mean value for homogenized, alkali-activated SM is 444.7 μm (standard deviation 178.4 μm). The value decreased by 15%, and the pores are more homogeneously distributed according to the decrease in standard deviation (1.5 times) compared to the mean value of the pore diameter (1.2 times). When comparing the EDXS results for intact and homogenized SM (Fig. 10 (b-element) and Fig. 11 (b-element) it can be concluded that after homogenization the distribution of the elements in the aluminosilicate network is somewhat more uniform.

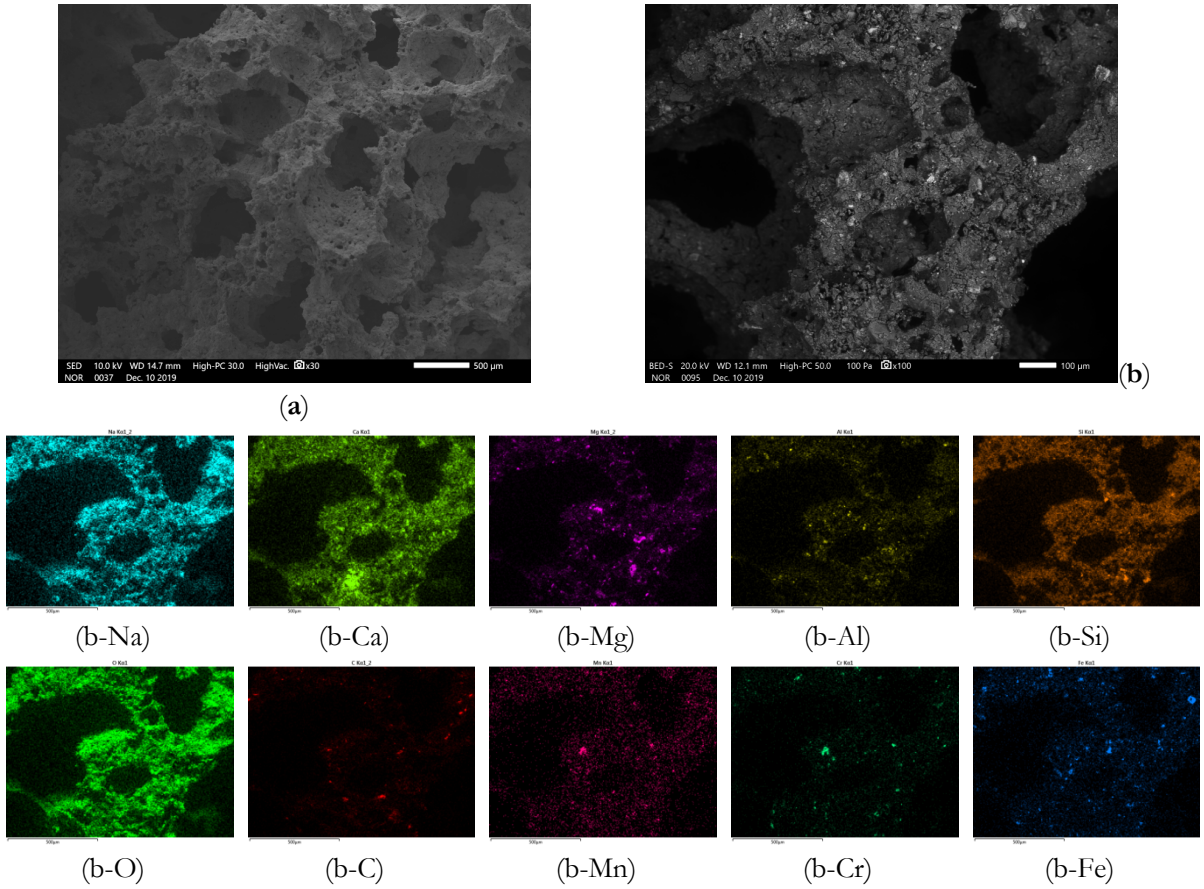

Figure 10: SEM micrograph of intact alkali-activated SM with magnification (a) 30 (intact cross-section after compressive strength test, vacuumed and sputtered with Au, observed at HV) and (b) 100 (cut and gently polished cross-section, observed at LV). The EDXS mapping of the micrograph (b) is presented on (b-chemical element). Source: own.

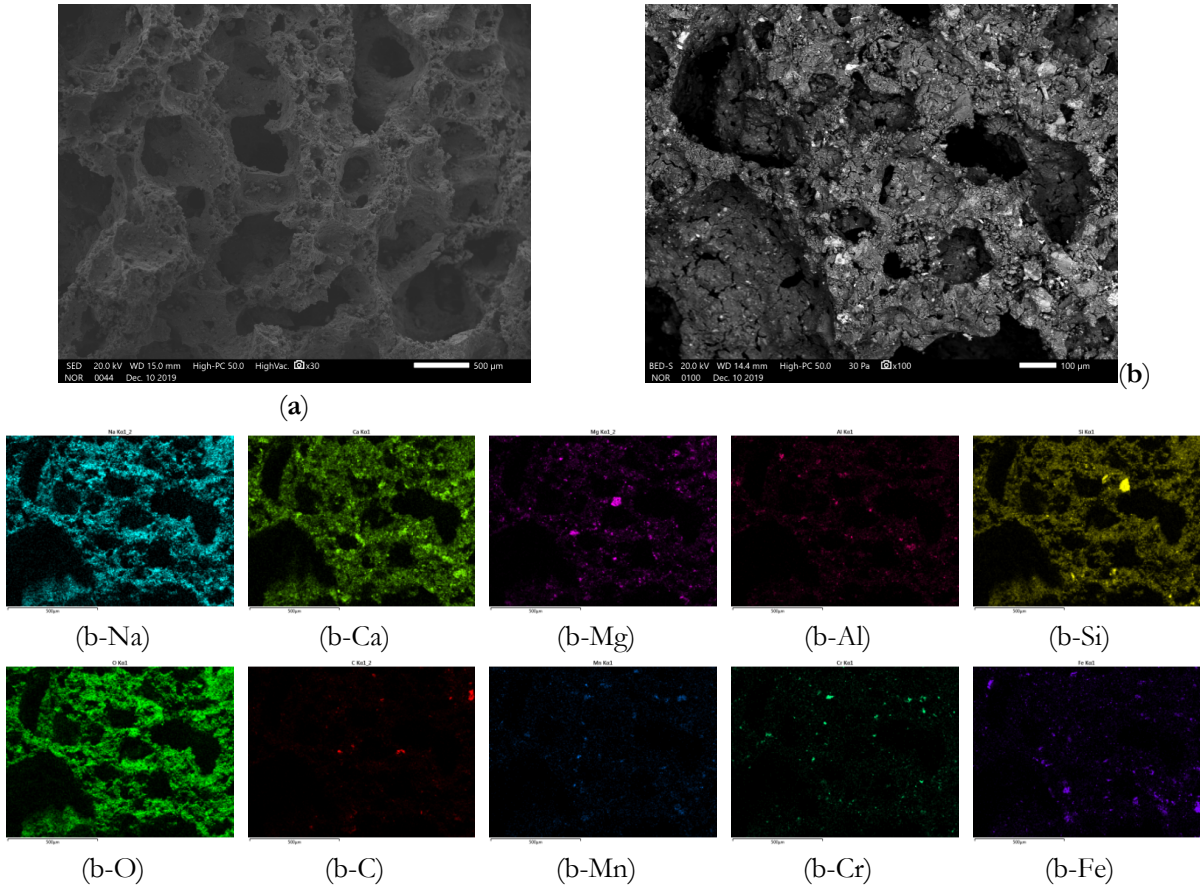

Figure 11: SEM micrograph of homogenized alkali-activated SM with magnification (a) 30 (intact cross-section after compressive strength test, vacuumed and sputtered with Au, observed at HV) and (b) 100 (cut and gently polished cross-section, observed at LV). The EDXS mapping of the micrograph (b) is presented on (b-chemical element. Source: own.

Fig. 12 shows intact alkali-activated GW and Fig. 13 shows homogenized alkali-activated GW.

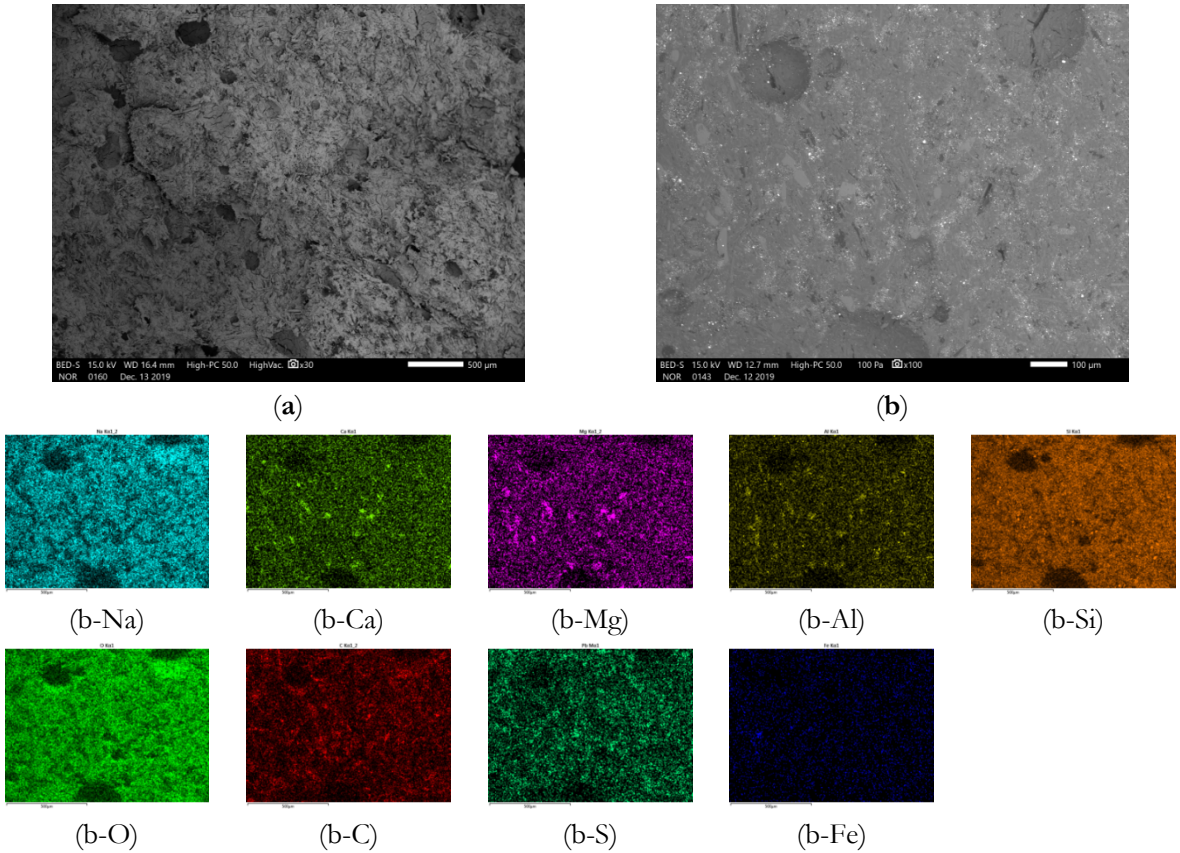

Figure 12: SEM micrograph of intact alkali-activated GW with magnification (a) 30 (intact cross-section after compressive strength test, vacuumed and sputtered with Au, observed at HV) and (b) 100 (cut and polished cross-section, observed at LV). The EDXS mapping of micrograph (b) is shown under (b-chemical element). Source: own.

The aluminosilicate network of GW with and without homogenization shows no visual difference (Fig. 12 (a) and Fig. 13 (a)), while from the EDXS analysis on the polished samples (Fig. 12 (b-element) and Fig. 13 (b-element)) it can be concluded that homogenization has a great influence on the distribution of the elements, which are somewhat more uniform in the homogenized sample.

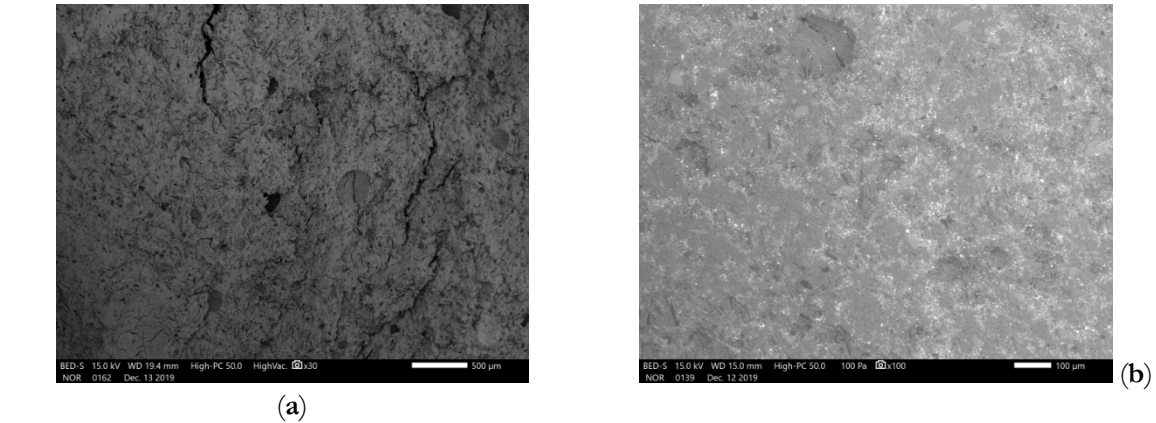

Figure 13: SEM micrograph of homogenized alkali-activated GW with magnification (a) 30 (intact cross-section after compressive strength test, vacuumed and sputtered with Au, observed at HV) and (b) 100 (cut and polished cross-section, observed at LV). The EDXS mapping of micrograph (b) is shown under (b-chemical element). Source: own.

Fig. 14 shows intact alkali-activated WGC and Fig. 15 homogenized alkali-activated WGC. There is no visual difference in the aluminosilicate network (Fig. 14 (a) and Fig. 15 (a)), while there is a difference in the distribution of the network due to bloating (non-thermally stable chemicals that change to gas when exposed to higher/high temperatures) after exposure to 105 °C for 24 h. In the intact sample bloating is less pronounced, random and with spherical bubbles, whereas in the homogenized sample is layered and perpendicular to the direction of moulding. From the EDXS analysis (Fig. 14 (b-element) and Fig. 15 (b-element), which was performed on polished samples and is shown in Fig. 14 (b) and Fig. 15 (b) respectively, it can be seen that the precursor itself was well homogenized, i.e. the distribution of the elements in the entire volume of the alkali-activated material is uniform with and without homogenization (EDXS sees no difference between unreacted and reacted parts of the alkali-activated WGC visible to the naked eye and shown in Fig. 4 (i) and (j)).

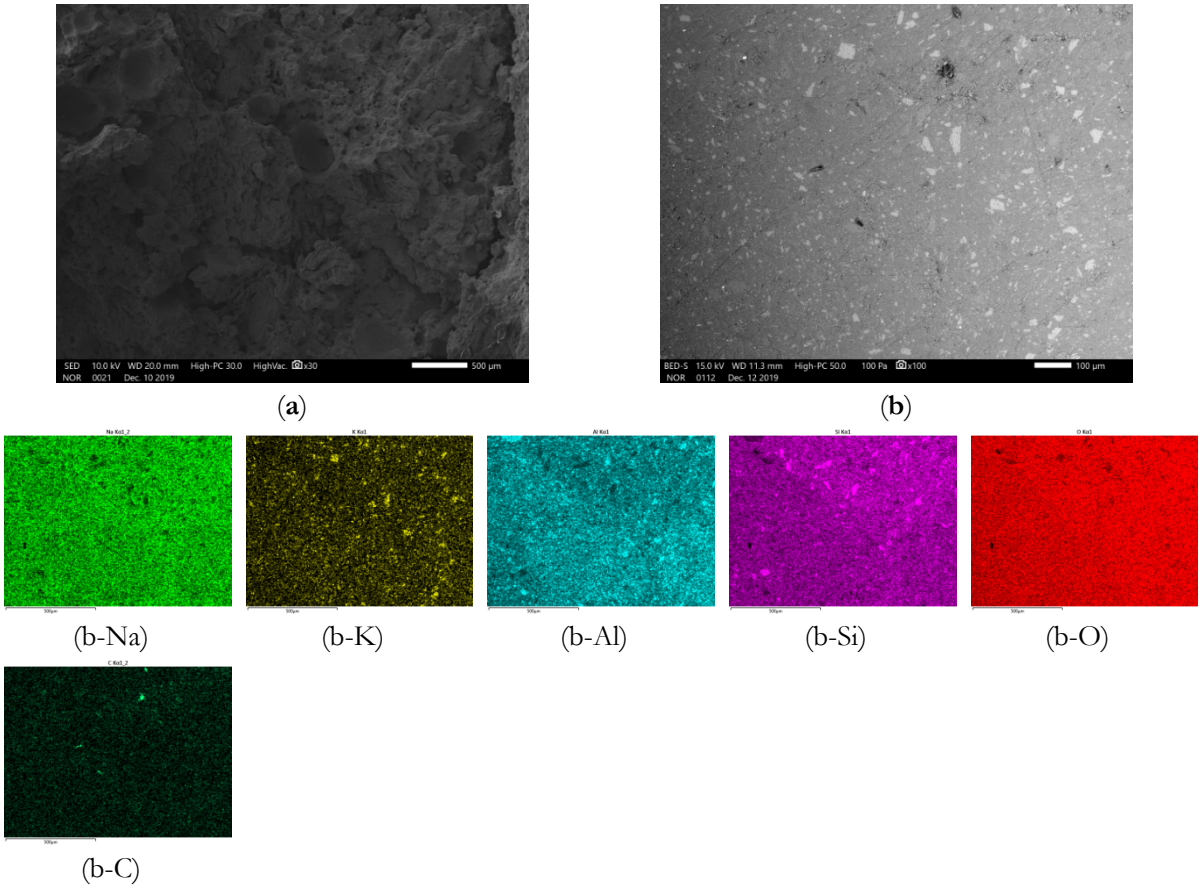

Figure 14: SEM micrograph of intact alkali-activated WGC with magnification (a) 30 (intact cross-section after compressive strength test, vacuumed and sputtered with Au, observed at HV) and (b) 100 (cut and polished cross-section, observed at LV). The EDXS mapping of the micrograph (b) is presented on (b-chemical element). Source: own.

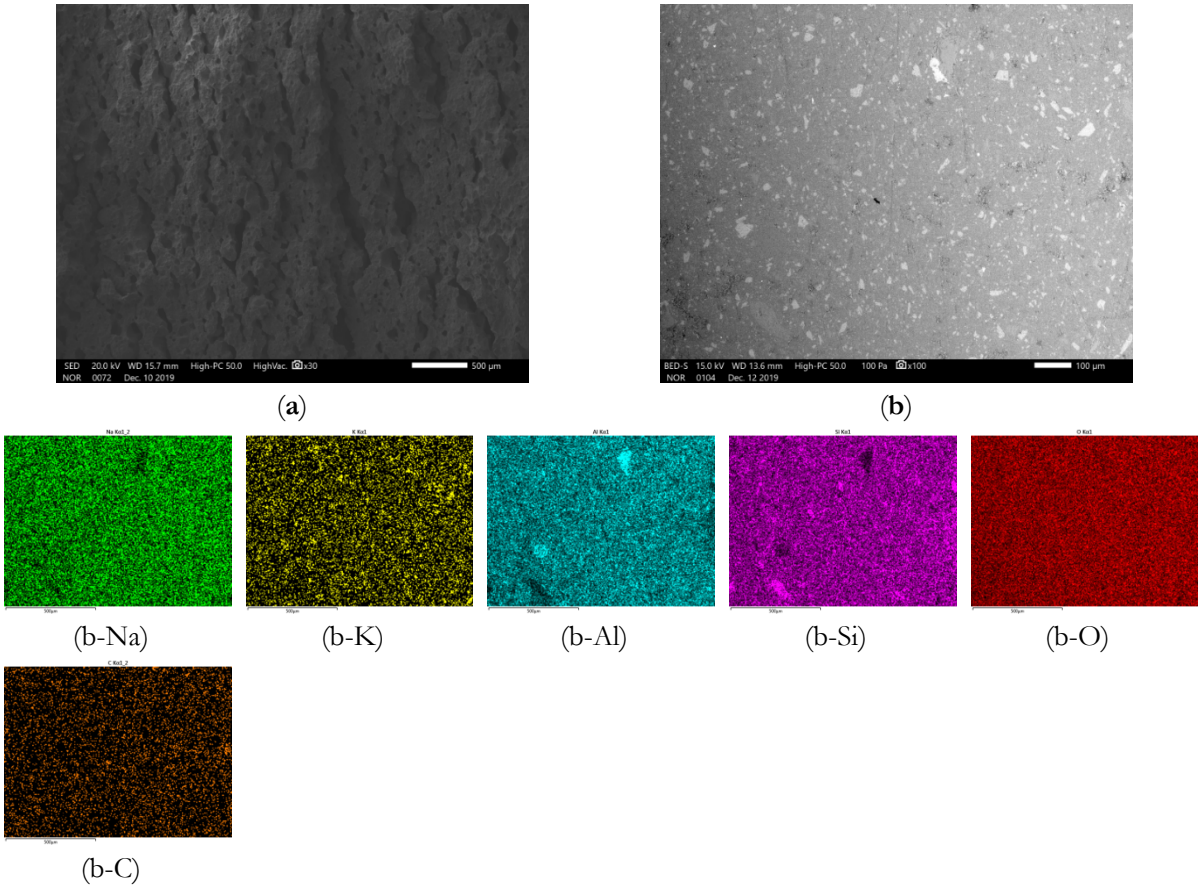

Figure 15: SEM micrograph of homogenized alkali-activated WGC with magnification (a) 30 (intact cross-section after compressive strength test, vacuumed and sputtered with Au, observed under HV; the direction of moulding is horizontal on the SEM micrograph) and (b) 100 (cut and polished cross-section observed under LV). The EDXS mapping of micrograph (b) is presented on (b-chemical element). Source: own.

4 Conclusions

The compressive and bending strength of alkali-activated material and alkali-activated foam were higher when the slurry was homogenized in its initial stage of reaction, regardless of other parameters influencing alkali activation, i.e. precursors, alkali activators, the ratio of ingredients, curing regimes and drying procedures. The increase in compressive strength was from 30% to 75%, the increase of bending strength from 10% to more than 100%. However, the homogenization of alkali-activated foam is only possible if the foaming agent has a delayed reaction with the reagents, i.e. when we are dealing with alkali-activated delayed foam, to avoid the increase in density of the foamed product due to the loss of gasses, which should be trapped in the alkali-activated precursor when the mixture is optimally designed.

The viscosity of the slurry was lower after homogenization, or at least it became measurable. The decrease was more than 50% for alkali-activated materials, whereas for alkali-activated foams the decrease in viscosity was just noticeable on an absolute scale. The density of alkali-activated materials did not change when alkali-activated material did not bloat after exposure to high temperatures (which has a negative effect on mechanical strength, as almost solid alkali-activated material turns into solid alkali-activated "foam"), or when alkali-activated foam had a delayed start of foaming.

In summary, it can be said that homogenization itself does not affect the alkali-activated reaction, it only affects the distribution of the elements and additionally grinds larger particles, resulting in a more reactive surface and a smaller volume of reagents that must dissolve before the liquid alkali can diffuse. In this way, homogenization helps to ensure that more precursor can react with alkali, which does not have to reach reagents only with "superficial" mixing of the reagents and later by time-limited diffusion in the slurry.

Acknowledgements

Project No. C3330-17-529032 "Raziskovalci-2.0-ZAG-529032" was granted by Ministry of Education, Science and Sport of the Republic of Slovenia. The investment is co-financed by the Republic of Slovenia, Ministry of Education, Science and Sport and the European Regional Development Fund. The involvement of V. Ducman was supported by the Slovenian Research Agency Programme Group P2-0273. The involvement of K. Traven and K. König was supported by Slovenian Research Agency

with Project Grant J2 9197. The involvement of M. Češnovar is part of the ERA-MIN FLOW project which has received funding from the Ministry of education, science and sport (acronym: MIZS) under grant agreement No. C 3330-18-252010. M. Pavlin is involved by the support of WOOL2LOOP project that received funding from the European Union's Horizon 2020 research and innovation programme under grant agreement No 821000.

The Metrology Institute of the Republic of Slovenia is acknowledged for the use of XRF.

Cooperation with Termit d.d. and Mrs Alenka Sešek Pavlin from Termit d.d.is highly appreciated.

References

Ahmed, M.H., Byrne, J.A., McLaughlin, J., Ahmed, W., 2013. Study of Human Serum Albumin Adsorption and Conformational Change on DLC and Silicon Doped DLC Using XPS and FTIR Spectroscopy. Journal of Biomaterials and Nanobiotechnology 04, 194–203. https://doi.org/10.4236/jbnb.2013.42024

Bernal, S.A., Provis, J.L., 2014. Durability of Alkali-Activated Materials: Progress and Perspectives. Journal of the American Ceramic Society 97, 997–1008. https://doi.org/10.1111/jace.12831

Češnovar, Traven, Horvat, Ducman, 2019. The Potential of Ladle Slag and Electric Arc Furnace Slag use in Synthesizing Alkali Activated Materials; the Influence of Curing on Mechanical Properties. Materials 12, 1173. https://doi.org/10.3390/ma12071173

Criado, M., Palomo, A., Fernández-Jiménez, A., Banfill, P.F.G., 2009. Alkali activated fly ash: effect of admixtures on paste rheology. Rheologica Acta 48, 447–455. https://doi.org/10.1007/s00397-008-0345-5

Duxson, P., Provis, J.L., Lukey, G.C., Mallicoat, S.W., Kriven, W.M., van Deventer, J.S.J., 2005. Understanding the relationship between geopolymer composition, microstructure and mechanical properties. Colloids and Surfaces A: Physicochemical and Engineering Aspects 269, 47–58. https://doi.org/10.1016/j.colsurfa.2005.06.060

Hajimohammadi, A., Ngo, T., Mendis, P., Sanjayan, J., 2017. Regulating the chemical foaming reaction to control the porosity of geopolymer foams. Materials & Design 120, 255–265. https://doi.org/10.1016/j.matdes.2017.02.026

Horvat, B., Češnovar, M., Pavlin, A., Ducman, V., 2018. Upcycling with alkali activation technology, in: Technologies & Business Models for Circular Economy. Presented at the 1st International Conference on Technologies & Business Models for Circular Economy, Univerzitetna založba Univerze v Mariboru / University of Maribor Press, pp. 261–272. https://doi.org/10.18690/978-961-286-211-4.22

Horvat, B., Ducman, V., 2019. Potential of Green Ceramics Waste for Alkali Activated Foams 30.

Hunger, M., Brouwers, H.J.H., 2009. Flow analysis of water–powder mixtures: Application to specific surface area and shape factor. Cement and Concrete Composites 31, 39–59. https://doi.org/10.1016/j.cemconcomp.2008.09.010

Juenger, M.C.G., Winnefeld, F., Provis, J.L., Ideker, J.H., 2011. Advances in alternative cementitious binders. Cement and Concrete Research 41, 1232–1243. https://doi.org/10.1016/j.cemconres.2010.11.012

Korat, L., Ducman, V., 2017. The influence of the stabilizing agent SDS on porosity development in alkali-activated fly-ash based foams. Cement and Concrete Composites 80, 168–174. https://doi.org/10.1016/j.cemconcomp.2017.03.010

Kramar, S., Šajna, A., Ducman, V., 2016. Assessment of alkali activated mortars based on different precursors with regard to their suitability for concrete repair. Construction and Building Materials 124, 937–944. https://doi.org/10.1016/j.conbuildmat.2016.08.018

Kutchko, B., Kim, A., 2006. Fly ash characterization by SEM–EDS. Fuel 85, 2537–2544. https://doi.org/10.1016/j.fuel.2006.05.016

Nematollahi, B., Ranade, R., Sanjayan, J., Ramakrishnan, S., 2017. Thermal and mechanical properties of sustainable lightweight strain hardening geopolymer composites. Archives of Civil and Mechanical Engineering 17, 55–64. https://doi.org/10.1016/j.acme.2016.08.002

Provis, J.L., Arbi, K., Bernal, S.A., Bondar, D., Buchwald, A., Castel, A., Chithiraputhiran, S., Cyr, M., Dehghan, A., Dombrowski-Daube, K., Dubey, A., Ducman, V., Gluth, G.J.G., Nanukuttan, S., Peterson, K., Puertas, F., van Riessen, A., Torres-Carrasco, M., Ye, G., Zuo, Y., 2019. RILEM TC 247-DTA round robin test: mix design and reproducibility of compressive strength of alkali-activated concretes. Materials and Structures 52. https://doi.org/10.1617/s11527-019-1396-z

Provis, J.L., Duxson, P., van Deventer, J.S.J., 2010. The role of particle technology in developing sustainable construction materials. Advanced Powder Technology 21, 2–7. https://doi.org/10.1016/j.apt.2009.10.006

Rajamma, R., Labrincha, J.A., Ferreira, V.M., 2012. Alkali activation of biomass fly ash–metakaolin blends. Fuel 98, 265–271. https://doi.org/10.1016/j.fuel.2012.04.006

Samson, G., Cyr, M., Gao, X.X., 2017. Thermomechanical performance of blended metakaolin-GGBS alkali-activated foam concrete. Construction and Building Materials 157, 982–993. https://doi.org/10.1016/j.conbuildmat.2017.09.146

Schlesinger, W.H., 1991. Biogeochemistry: an analysis of global change. Academic Press, San Diego.

Traven, K., Češnovar, M., Ducman, V., 2019. Particle size manipulation as an influential parameter in the development of mechanical properties in electric arc furnace slag-based AAM. Ceramics International. https://doi.org/10.1016/j.ceramint.2019.07.296

Traven, K., Črešnovar, M., Škapin, S., Ducman, V., 2020. Evaluation of Fly Ash-based Alkali Activated Foams at Room and Elevated Temperatures, in: 2nd International Conference on : Technologies & Business Models for Circular Economy: Conference Proceedings. Presented at the International Conference on Technologies & Business Models for Circular Economy, University of Maribor, University Press, pp. 23–34. https://doi.org/10.18690/978-961-286-353-1.2

Van Deventer, J.S.J., Provis, J.L., Duxson, P., 2012. Technical and commercial progress in the adoption of geopolymer cement. Minerals Engineering 29, 89–104. https://doi.org/10.1016/j.mineng.2011.09.009

Vlček, J., Drongová, L., Topinková, M., Matějka, V., Kukutschová, J., Vavro, M., Tomková, V., 2014. Identification of phase composition of binders from alkali-activated mixtures of granulated blast furnace slag and fly ash 10.